Identification and analysis of immunological characteristics of prognostic feature for osteosarcoma based on costimulatory molecule-related genes

Keywords
Osteosarcoma, Costimulatory molecule, prognostic gene signature, Immunological characteristics

Abstract

Introduction
Osteosarcoma (OSA) is a primary malignant bone tumor with poor prognosis. Costimulatory molecule-related genes (CMRGs) are crucial for T cell-mediated antitumor immunity, yet their prognostic and therapeutic value in OSA remains unclear.

Material and methods
Non-negative matrix factorization (NMF) clustering was used to define CMRG-based subtypes. Prognostic signature genes were selected using univariate Cox, LASSO, and multivariate regression analyses. The predictive performance of the model was assessed using ROC curves, calibration plots, and decision curve analysis (DCA). Immune infiltration and immune checkpoint differences were evaluated via ssGSEA. Drug sensitivity was predicted using CellMiner, and gene expression was validated by qRT-PCR in OSA cells.

Results
This study selected five characteristic genes related to the prognosis of OSA and constructed a prognostic model. The evaluation results indicate that the model has favorable predictive performance, with calibration curves and DCA confirming that the predicted survival probabilities aligned with the actual survival probabilities of patients. Furthermore, the response results for immunotherapy revealed that patients with lower risk scores had more favorable immune responses and lower rates of disease metastasis. Notably, DMAPT, Obatoclax, 8-Chloro-adenosine, and Palbociclib showed a significant positive correlation with MYC. Additionally, qRT-PCR results indicated that EPYC, SCD1, and AOC3 were significantly overexpressed in OSA cells.

Conclusions
This study is the first to integrate CMRG-based subtyping, risk modeling, immune profiling, and experimental validation in OSA. The identified biomarkers may guide personalized treatment and improve survival prediction in OSA patients.

Identification and analysis of immunological characteristics of prognostic feature for osteosarcoma based on costimulatory molecule-related genes

Abstract

Background

Osteosarcoma (OSA) is a primary malignant bone tumor with poor prognosis. Costimulatory molecule-related genes (CMRGs) are crucial for T cell-mediated antitumor immunity, yet their prognostic and therapeutic value in OSA remains unclear.

Methods

Non-negative matrix factorization (NMF) clustering was used to define CMRG-based subtypes. Prognostic signature genes were selected using univariate Cox, LASSO, and multivariate regression analyses. The predictive performance of the model was assessed using ROC curves, calibration plots, and decision curve analysis (DCA). Immune infiltration and immune checkpoint differences were evaluated via ssGSEA. Drug sensitivity was predicted using CellMiner, and gene expression was validated by qRT-PCR in OSA cells.

Results

This study selected five characteristic genes related to the prognosis of OSA and constructed a prognostic model. The evaluation results indicate that the model has favorable predictive performance, with calibration curves and DCA confirming that the predicted survival probabilities aligned with the actual survival probabilities of patients. Furthermore, the response results for immunotherapy revealed that patients with lower risk scores had more favorable immune responses and lower rates of disease metastasis. Notably, DMAPT, Obatoclax, 8-Chloro-adenosine, and Palbociclib showed a significant positive correlation with MYC. Additionally, qRT-PCR results indicated that EPYC, SCD1, and AOC3 were significantly overexpressed in OSA cells.

Conclusion

This study is the first to integrate CMRG-based subtyping, risk modeling, immune profiling, and experimental validation in OSA. The identified biomarkers may guide personalized treatment and improve survival prediction in OSA patients.

Key words: Osteosarcoma, Costimulatory molecule, prognostic gene signature, Immunological characteristics

1.Introduction

Osteosarcoma (OSA) is a highly aggressive primary malignant bone tumor originating from mesenchymal cells, predominantly affecting children and adolescents [1]. It is characterized by a high propensity for early metastasis, particularly to the lungs, contributing to poor prognosis [2, 3]. While localized OSA has a five-year survival rate of ~60%, this rate drops to ~20% in metastatic cases [4, 5]. Despite surgical and chemotherapeutic advances, overall survival has not significantly improved over the past two decades [6], largely due to tumor heterogeneity, genetic alterations, and chemoresistance [7-9].

Recent studies have highlighted that non-coding RNAs and epigenetic modifications are crucial contributors to OSA chemoresistance. For instance, METTL3-mediated m6A methylation stabilizes LINC00520, which enhances glycolysis and cisplatin resistance by stabilizing ENO1 protein [10]. In addition, ferroptosis has emerged as a key mechanism in OSA progression and therapy response. Exosome-mediated delivery of miR-144-3p was shown to inhibit OSA cell proliferation and invasion by promoting ferroptosis through ZEB1 suppression [11].

Moreover, dysregulated cell death pathways such as autophagy and ferroptosis may be therapeutically exploitable. Overexpression of Apolipoprotein E (APOE) has been reported to suppress OSA growth by inducing both autophagy and ferroptosis via inhibition of the mTOR/Stat3 signaling pathway [12]. These findings underscore the need for better prognostic markers and novel therapeutic strategies in OSA.

The tumor microenvironment (TME)—comprising tumor cells, immune cells, stromal components, and cytokines—plays a critical role in cancer progression, metastasis, and immunotherapy efficacy [13]. In this context, costimulatory molecules are essential in mediating T cell activation and immune modulation [8, 14, 15]. These molecules, primarily from the B7-CD28 and TNF superfamilies, are involved in delivering the second signal required for effective T cell responses [16-21]. While studies have implicated B7 family members such as PD-L1 and B7-H1 in OSA immune regulation [18], a comprehensive understanding of costimulatory

molecule-related genes (CMRGs) in OSA remains lacking.

To address this, we conducted a systematic analysis of CMRG expression patterns, identified molecular subtypes, and developed a prognostic model using characteristic CMRGs. We further evaluated immune infiltration, predicted drug sensitivity, and validated key genes via qRT-PCR. This integrative approach aims to elucidate the immunological and prognostic significance of CMRGs in OSA and to support the development of individualized treatment strategies.

2.Materials and methods

2.1 Data origin

mRNA expression data related to TARGET-OS were retrieved from the TCGA database (https://portal.gdc.cancer.gov/). Patient clinical information was sourced from the TARGET database (https://ocg.cancer.gov/programs/target). Additionally, microarray datasets were obtained from the Gene Expression Omnibus (GEO) database (GSE21257 and GSE99671), while single-cell data came from GSE152048. To identify 60 CMRGs, we reviewed existing literature (Supplementary Table S1, TS1) [22]. The IMvigor210CoreBiologies package was employed to gather data on immunotherapy cohorts and relevant clinical details for bladder cancer (BLCA) patients undergoing immune checkpoint therapy.

2.2 Differential analysis and molecular subtype construction based on CMRGs

Using the "edgeR" package, differential analysis was performed on the GSE99671 dataset, comparing the normal group (N=18) and the tumor group (OSA, N=18) with criteria of |log Fold change (FC)| > 0.585 and $P < 0.05$. The differentially expressed genes (OSA-DEGs) were intersected with CMRGs, resulting in CMRG-related differentially expressed genes (DECMRGs, Supplementary Table S2，TS2). The expression levels of the DECMRGs in both the normal and tumor groups were quantified, and a heatmap was generated. Based on the DECMRGs, the Non-negative Matrix Factorization (NMF) clustering method was employed to classify the TARGET-OS dataset. Survival analysis of the three subtypes was conducted using Kaplan-Meier (K-M) curves.

2.3 Immune status analysis of molecular subtypes

Using the "GSVA" package, single-sample Gene Set Enrichment Analysis (ssGSEA) analysis was conducted to investigate the differences in immune-related

functions and immune cell infiltration among the three subtypes. The ESTIMATE algorithm was employed to evaluate the stromal score, immune score, ESTIMATE score and tumor purity for each sample across the three subtypes. Clusters 2 and 3 were merged to form a new subtype. Subsequently, the "clusterProfiler" package was utilized to perform Gene Ontology (GO) and Kyoto Encyclopedia of Genes and Genomes (KEGG) enrichment analysis on the differentially expressed genes (group-DEGs) between Cluster 1 and the merged subtype (Supplementary Table S3, TS3).

2.4 Selection of prognostic feature genes for OSA and construction of a prognostic model

Clinical data were merged with the expression levels of differentially expressed genes. The intersection of group-DEGs (|logFC| > 1, $P < 0.01$) and OSA-DEGs (|logFC| > 0.585, $P < 0.05$) was used as candidate genes. To prevent model overfitting, Least Absolute Shrinkage and Selection Operator (LASSO) regression analysis was performed on the candidate genes using the "glmnet" package. Cross-validation was employed to select the penalty parameter lambda, which helped eliminate highly correlated genes and reduce model complexity. A multivariate regression analysis of the candidate genes was conducted using the "survival" package to construct the prognostic model.

Risk score=$\sum_{i=1}^{n} \beta i * Expi$. βi is the risk coefficient, and $Expi$ is the gene expression level.

Based on this model, a risk score for each patient was calculated using the expression levels and risk coefficients of the genes, where the risk score was categorized into high- and low-risk groups according to the median score. Survival curves were generated based on the risk scores. The "timeROC" package was used to plot Receiver Operating Characteristic (ROC) curves and calculate the Area Under the Curve (AUC) values for 1-year, 3-year, and 5-year survival rates. Additionally, score distribution plots, survival status distribution plots, and heatmaps of expression levels were created for the high- and low-risk groups.

2.5 Construct a nomogram for independent prognostic analysis

We conducted univariate and multivariate regression analyses on the training set samples, integrating clinical information and prognostic risk scores, and generated corresponding forest plots. Utilizing the "rms" package, we constructed a nomogram

to predict patient survival rates at 1, 3, and 5 years. Calibration curves and decision curve analysis (DCA) curves were subsequently plotted to assess the predictive performance of the nomogram and to establish its role as an independent prognostic factor. Furthermore, we validated the predictive accuracy of the nomogram using calibration curves derived from the independent dataset GSE21257.

2.6 Immunological evaluation

We employed “GSVA” and the “estimate” package to conduct ssGSEA analysis, quantifying the extent of immune cell infiltration. Violin plots were generated to illustrate immune scores, stromal scores, ESTIMATE scores, and tumor purity for both high- and low-risk groups. Box plots were created to statistically compare the expression levels of immune checkpoints and the degree of immune cell infiltration between these groups. The Tumor Immune Phenotype (TIP) (http://biocc.hrbmu.edu.cn/TIP/) is a web-based analysis platform designed to assess the activation levels of the seven steps in the anti-cancer immune cycle [23]. We evaluated the correlation between the activation levels of this immune cycle and risk scores, along with characteristic genes. Furthermore, we utilized the ssGSEA algorithm, TIMER algorithm, and MCP-Counter to analyze the relationships between characteristic genes and immune cells.

2.7 Investigation of biological functions and active pathways

Differential analysis was performed on the high-risk and low-risk groups of OSA using the edgeR package ($|logFC|>1$, $P<0.05$). GO and KEGG enrichment analyses were conducted on the differentially expressed genes using the "clusterProfiler" package and "GOplot."

2.8 Analyzing the efficacy of risk scores in predicting immune therapy response

Anti-PD-1 and anti-PD-L1 checkpoint inhibitor therapies have emerged as significant components of immunotherapy, garnering considerable attention [24]. To assess the efficacy of risk scores in predicting responses to immune checkpoint blockade, we gathered transcriptomic and clinical data from patients receiving anti-PD-L1 treatment within the IMvigor210 cohort (Supplementary Table S4, TS4). Utilizing the risk scores, we categorized the samples into high-risk and low-risk groups.

2.9 Single-cell sequencing analysis based on OSA

This study employed the Read10X function from the “Seurat” package to analyze gene expression data from 11 samples in GSE152048. We identified the top

2,000 highly variable genes using the FindVariableFeatures function, and removed batch effects through anchor-based data integration with the FindIntegrationAnchors function. Low-quality cells, defined as those with fewer than 300 detected genes or exhibiting more than 10% mitochondrial gene expression, were excluded and normalized. Utilizing the "SCISSOR" package, we categorized cells into high-risk and low-risk groups based on patient expression data and risk stratification information from TARGET-OS. Finally, we analyzed and visualized the intercellular communication network within the TME using the "CellChatR" package.

2.10 Potential drug targets and prediction of drug inhibitory concentrations

The present study aimed to identify new potential targets and more effective therapeutic agents. We utilized the CellMiner database (https://discover.nci.nih.gov/cellminer/) to screen for antitumor drugs significantly associated with sensitivity and prognostic genes. Additionally, we explored the DGIdb database (https://www.dgidb.org) to identify approved drugs that interact with the feature genes, discussing the potential drug targets and mechanisms linked to disease susceptibility genes. The "pRRophetic" package was employed to predict the half-maximal inhibitory concentration (IC50) of various drugs in high-risk and low-risk groups. A lower IC50 indicates greater effectiveness of the drug in tumor treatment.

2.11 Cell acquisition and cell culture

hFOB1.19, SAOS2 and U2OS cell lines were obtained from the American Type Culture Collection (ATCC) and cultured in DMEM medium. All cell cultures were maintained in a 37° C incubator with 5% CO_2.

2.12 RNA isolation and quantitative real-time PCR (qRT-PCR)

Total RNA was extracted from cells using RNAiso Trizol reagent (Sangon Biotech, China). cDNA was synthesized through reverse transcription with the GeniuSaript III Select RT Kit for qPCR (Youji, China). For qRT-PCR, the uGreener Fex qPCR 2X MiX (Youji, China) was utilized on the LightCycler 480 qPCR system (Roche, Switzerland), with the primer sequences listed below. The results were normalized to GAPDH, and relative expression levels were calculated using the $2^{-\Delta\Delta CT}$ method.

Gene name	Forward primer sequence (5'-3')	Reverse primer sequence (5'-3')
EPYC	AGGTCAGAGCCAAAGGAAAGC	TAGAGTTGGGGCAGTCACAG

SCD1	TTCCCGACGTGGCTTTTTCT	AGCCAGGTTTGTAGTACCTCC
AOC3	CAAGTGTCAGAGCACACCCT	TCCAGTCCTGCTACATCCAGA
MYC	TGGAAAACCAGCCTCCCG	TTCTCCTCCTCGTCGCAGTA
KLK2	TGGAGGGGAAAGGGTGATTC	CCACTTCCGGTAATGCACCA
GAPDH	ACATCGCTCAGACACCATG	TGTAGTTGAGGTCAATGAAGGG

2.13 Cytotoxicity Assay

Using the 3-(4, 5-dimethylthiazol-2-yl)-2, 5-diphenyltetrazolium bromide (MTT) method to determine the toxic effects of drugs on cells. U2OS and SAOS2 cells were seeded into a 96 well plate. After cell attachment, the cells were treated with various concentrations of Temozolomide or Cisplatin for 48 hours, including a blank control group. Subsequently, 10 μL of MTT solution was added to each well and the plate was incubated at 37°C for 2 hours. The supernatant was then aspirated, and DMSO was added to dissolve the formazan. The absorbance of each well was measured at a wavelength of 490 nm.

2.14 Cell apoptosis assay

Using terminal deoxynucleotidyl transferase (TdT) dUTP nick-end labeling (TUNEL) assay to assess the effect of drugs on cell apoptosis. Seed U2OS and SAOS2 cells onto culture plates containing coverslips. After cell attachment, treat cells with Temozolomide or Cisplatin for 48 hours, including a solvent control group. Following treatment, perform TUNEL staining: fix cells with 4% paraformaldehyde, permeabilize with 0.1% Triton X-100, incubate with TUNEL reaction mixture to label DNA fragmentation, and counterstain nuclei with DAPI. After washing steps, mount coverslips with antifade mounting medium and observe under a fluorescence microscope. Randomly select multiple fields of view, count the number of TUNEL positive cell and DAPI positive cell, and calculate the apoptosis rate.

3.Results

3.1 Identification of CMRGs linked to OSA and development of molecular subtypes from DECMRGs

This study initially conducted a differential analysis of the normal and OSA groups in the GSE99671 dataset (Normal: 18, OSA: 18) with criteria set at $|logFC| > 0.585$ and $P < 0.05$, resulting in 1,046 upregulated and 1,365 downregulated genes (OSA-DEGs, Figure 1A). By intersecting OSA-DEGs with CMRGs, we identified 13

differentially expressed CMRG-related genes (DECMRGs, Figure 1B). A PPI network was constructed for the 13 DECMRGs using the STRING database, as illustrated in Figure 1C, revealing strong interactions among CTLA4, TNFRSF4, CD86, CD276, and CD28. The expression levels of DECMRGs in both the normal and OSA groups were analyzed, and a heatmap was generated, indicating that CTLA4, TNFRSF4, CD86, CD276, and CD28 were significantly overexpressed in the OSA group (Figure 1D).

The objective of this study was to conduct a comprehensive analysis of the key characteristics of OSA tissues to inform the design of personalized treatment strategies for OSA patients. To accomplish this, we utilized NMF clustering techniques to classify the TARGET-OS samples into three subtypes based on DECMRGs (Sample: Cluster 1: 26, Cluster 2: 13, Cluster 3: 46, Figure 1E). K-M curve analysis demonstrated significant differences in survival outcomes among the three subtypes, with Cluster 1 showing the poorest survival rates (Figure 1F).

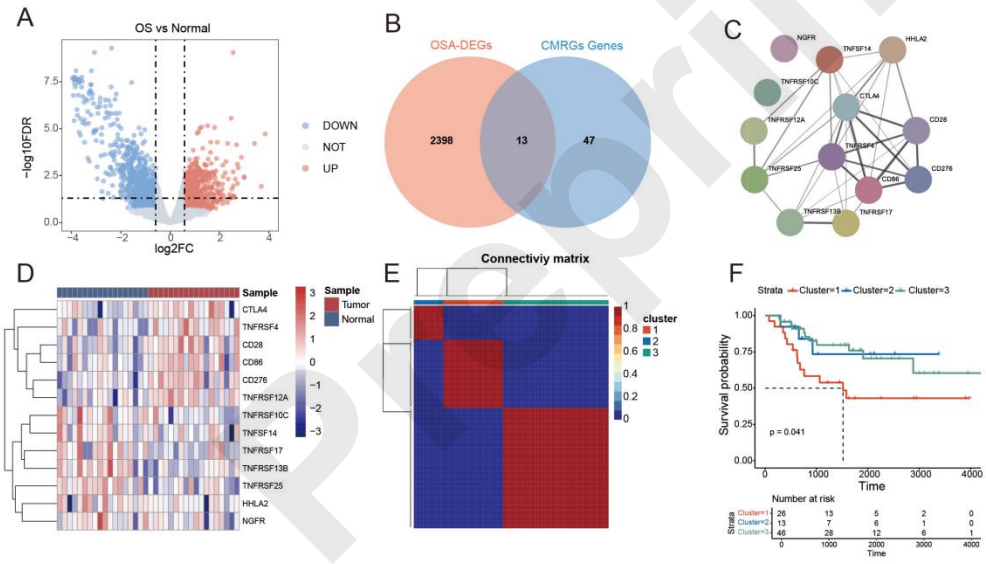

Figure 1 Identification of prognostic candidate genes and subtype construction. (A) The volcano plot depicts the expression of differentially expressed genes between normal tissue and OSA tissue, (upregulated: 1046, downregulated: 1365). (B) The Venn diagram shows the intersecting genes between OSA-DEGs and CMRGs gene sets. (C) The results of the PPI network diagram for the 13 DECMRGs. (D) Heatmap showing the differences in expression of the 13 DECMRGs in normal and OSA tissues. (E) NMF clustering results show that the optimal number of clustering results is 3. (F) K-M curve analysis describes the survival outcomes for the three

subgroups of patients, with those in subtype 1 having the poorest survival.

3.2 Analysis of immune function and immune cell infiltration among molecular subtypes based on DECMRGs

To explore the differences in immune-related functions and immune cell infiltration among the three subtypes, we conducted ssGSEA analysis to evaluate immune cell infiltration across these subtypes (Figure 2A). Our findings indicate that subtype 3 exhibited significantly higher levels of immune cell infiltration compared to subtypes 1 and 2. The results illustrated in Figures 2B and 2C further confirm that immune cell infiltration is notably more pronounced in subtype 3. Furthermore, stromal score comparisons revealed that subtype 3 had a significantly higher stromal score than subtype 1 (P=0.0085). In contrast, subtype 1 exhibited significantly higher tumor purity than subtype 3 (P=0.049), while its ESTIMATE score was significantly lower than that of subtype 3 (P=0.049) (Figure 2D).

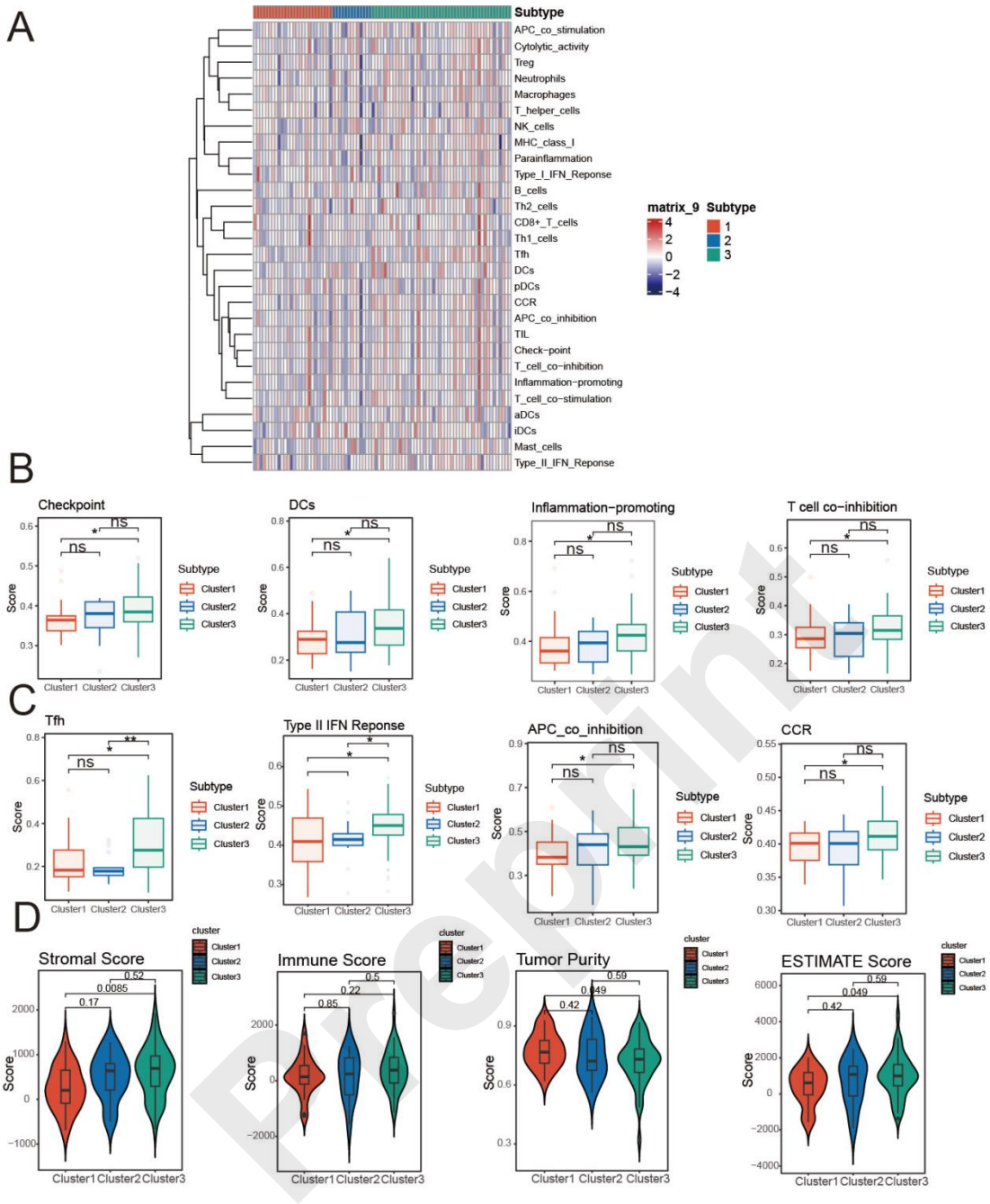

Figure 2 Analysis of immune function and immune infiltration. (A) The heatmap depicts the differences in immune cell infiltration in the three subtypes groups. (B) Box plots show analysis of differences in the degree of infiltration of each immune cell in the three subtyping groups. (C) Variations in immune cell infiltration among the three subtypes. (D) The violin plot illustrates the findings related to the Stromal score, immune score, tumor purity, and ESTIMATE score across the three subtypes. ns denotes no significant difference, * signifies $P<0.05$, ** represents $P<0.01$, and *** corresponds to $P<0.001$.

3.3 Differential analysis and biological function exploration among subtypes

We analyzed DECMRG expression across the three subtypes and found that

TNFRSF12A showed the lowest expression in subtype 1, while NGFR was significantly higher in subtype 2 compared to the other subtypes. Additionally, CD276 was most highly expressed in subtype 1, and TNFRSF10C was most highly expressed in subtype 3 (Figure 3A). To further investigate the clinical characteristics of the three patient subtypes, we conducted a statistical analysis of disease metastasis. As shown in Figure 3B, the metastasis rates were 23% in subtype 1, 15% in subtype 2, and 28% in subtype 3. To explore differences between the subtypes, we merged the data from subtypes 2 and 3 based on survival outcomes. We then performed a differential analysis of the combined gene set against subtype 1, using thresholds of log|FC|>1 and P <0.01. This yielded 1,187 differentially expressed genes (group-DEGs), including 802 upregulated and 385 downregulated genes (Figure 3C). Subsequently, we conducted GO and KEGG analyses to further explore the biological functions and pathway activities associated with the groups-DEGs. As illustrated in Figure 3D, upregulated genes were enriched in extracellular structure and muscle tissue-related processes. In contrast, downregulated genes were mainly associated with neuroregulation, transmembrane transport, and protein function (Figure 3E). KEGG analysis showed that upregulated genes were significantly involved in neural activity regulation, inflammatory signaling, and protein metabolism-related pathways (Figure 3F), while downregulated genes were primarily enriched in protein metabolism-related pathways (Figure 3G).

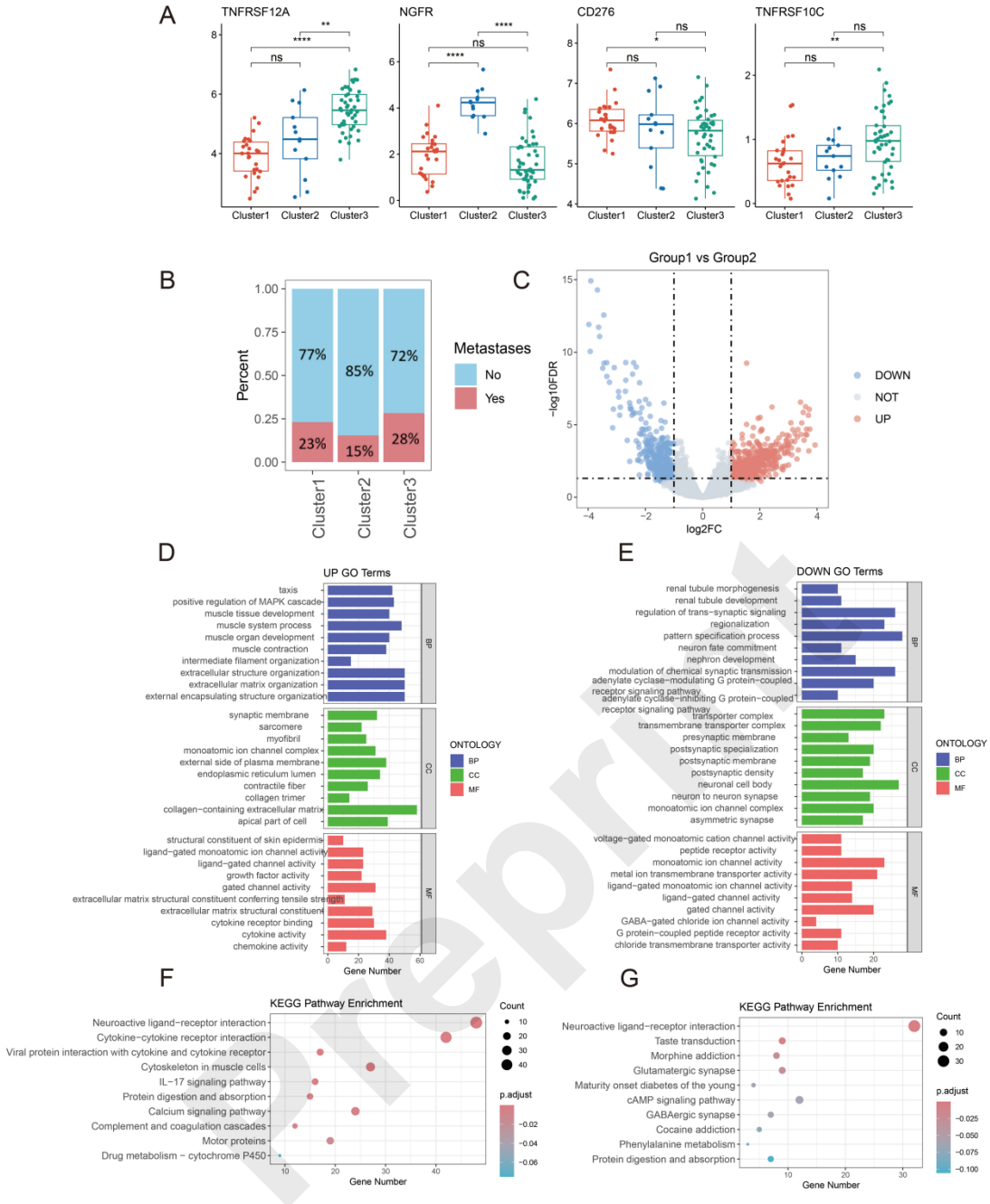

Figure 3 Analysis of differences between subtypes and functional exploration. (A) The analysis of DECMRG expression among subtypes shows expression levels plotted on the vertical axis, while the horizontal axis represents the different subtypes groups. (B) Metastasis of illness in patients with various subtypes. (C) The volcano plot represents the number of differentially expressed genes between the merged subtypes (subtype 2 and 3) and subtype 1, upregulated genes: 802, downregulated genes: 385. (D) Results of GO enriching of upregulated genes. (E) The findings of GO enriching of downregulated genes. (F) KEGG enrichment analysis for elevated gene expression. (G) Outcomes of KEGG enrichment for downregulated genes. ns indicates no significant difference, * indicates significant difference, ** indicates more significant, and *** indicates highly significant.

3.4 Identification of prognosis-related feature genes for developing OSA prognosis models

To further analyze the prognostic characteristics of OSA, this study identified the intersection of the OSA-DEGs gene set and the group-DEGs gene set, resulting in 274 overlapping genes (Figure 4A). Subsequently, univariate Cox analysis was performed, which yielded 54 genes significantly associated with survival ($P < 0.05$) (Figure 4B). LASSO regression analysis was then employed to refine the list of candidate genes (Figure 4C). Based on cross-validation results, we selected an optimal model with 13 genes (Figure 4D). Further multivariate regression analysis resulted in the selection of 5 characteristic genes to construct the prognostic model: risk score = -0.3182*EPYC + 0.2907*SCD1 + 0.5353*AOC3 + 0.6530*MYC + 2.0331*KLK2 (Figure 4E). To evaluate model accuracy, ROC curves were plotted. As shown in Figure 4F, the AUC values for the training set were 0.895 (1 year), 0.834 (3 years), and 0.862 (5 years). For the validation set, the AUCs were 0.719, 0.714, and 0.698 at the respective time points (Figure 4G). These results indicate excellent predictive performance. Based on the median risk score, OSA patients were classified into low-risk and high-risk groups. As illustrated in the K-M curve results in Figure 4H, the survival rate of patients in the low-risk group was significantly higher than that of the high-risk group ($P < 0.0001$). Additionally, survival status and risk scores were more favorable in the low-risk group (Figure 4I). Among the feature genes, SCD1, MYC, AOC3, and KLK2 were overexpressed in the high-risk group, while EPYC was expressed at lower levels (Figure 4J).

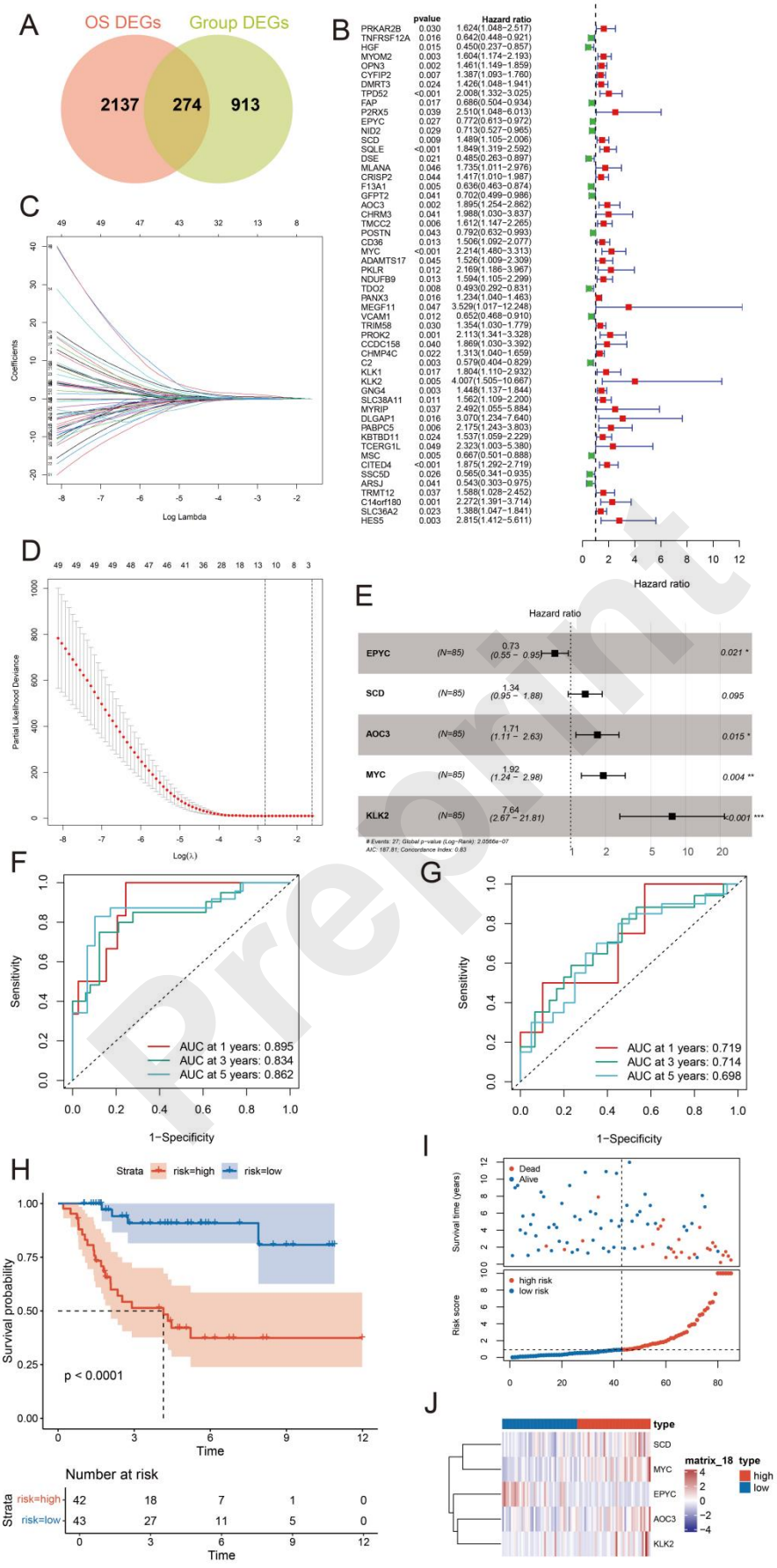
A
OS DEGs
Group DEGs
2137
274
913
B
pvalue
Hazard ratio
PRKAR2B 0.030 1.624(1.048−2.517)
TNFRSF12A 0.016 0.642(0.448−0.921)
HGF 0.015 0.450(0.237−0.857)
MYOM2 0.003 1.604(1.174−2.193)
OPN3 0.002 1.461(1.149−1.859)
CYFIP2 0.007 1.387(1.093−1.760)
DMRT3 0.024 1.426(1.048−1.941)
TPD52 <0.001 2.008(1.332−3.025)
FAP 0.017 0.686(0.504−0.934)
P2RX5 0.039 2.510(1.048−6.013)
EPYC 0.027 0.772(0.613−0.972)
NID2 0.029 0.713(0.527−0.965)
SCD 0.009 1.489(1.105−2.006)
SQLE <0.001 1.849(1.319−2.592)
DSE 0.021 0.485(0.263−0.897)
MLANA 0.046 1.735(1.011−2.976)
CRISP2 0.044 1.417(1.010−1.987)
F13A1 0.005 0.636(0.463−0.874)
GFPT2 0.041 0.702(0.499−0.986)
AOC3 0.002 1.895(1.254−2.862)
CHRM3 0.041 1.988(1.030−3.837)
TMCC2 0.006 1.612(1.147−2.265)
POSTN 0.043 0.792(0.632−0.993)
CD36 0.013 1.506(1.092−2.077)
MYC <0.001 2.214(1.480−3.313)
ADAMTS17 0.045 1.526(1.009−2.309)
PKLR 0.012 2.169(1.186−3.967)
NDUFB9 0.013 1.594(1.105−2.299)
TDO2 0.008 0.493(0.292−0.831)
PANX3 0.016 1.234(1.040−1.463)
MEGF11 0.047 3.529(1.017−12.248)
VCAM1 0.012 0.652(0.468−0.910)
TRIM58 0.030 1.354(1.030−1.779)
PROK2 0.001 2.113(1.341−3.328)
CCDC158 0.040 1.869(1.030−3.392)
CHMP4C 0.022 1.313(1.040−1.659)
C2 0.003 0.579(0.404−0.829)
KLK1 0.017 1.804(1.110−2.932)
KLK2 0.005 4.007(1.505−10.667)
GNG4 0.003 1.448(1.137−1.844)
SLC38A11 0.011 1.562(1.109−2.200)
MYRIP 0.037 2.492(1.055−5.884)
DLGAP1 0.016 3.070(1.234−7.640)
PABPC5 0.006 2.175(1.243−3.803)
KBTBD11 0.024 1.537(1.059−2.229)
TCERG1L 0.049 2.323(1.003−5.380)
MSC 0.005 0.667(0.501−0.888)
CITED4 <0.001 1.875(1.292−2.719)
SSC5D 0.026 0.565(0.341−0.935)
ARSJ 0.041 0.543(0.303−0.975)
TRMT12 0.037 1.588(1.028−2.452)
C14orf180 0.001 2.272(1.391−3.714)
SLC36A2 0.023 1.388(1.047−1.841)
HES5 0.003 2.815(1.412−5.611)
Hazard ratio
C
Coefficients
Log Lambda
D
Partial Likelihood Deviance
Log(λ)
E
Hazard ratio
EPYC (N=85) 0.73 (0.55 − 0.95) 0.021 *
SCD (N=85) 1.34 (0.95 − 1.88) 0.095
AOC3 (N=85) 1.71 (1.11 − 2.63) 0.015 *
MYC (N=85) 1.92 (1.24 − 2.98) 0.004 **
KLK2 (N=85) 7.64 (2.67 − 21.81) <0.001 ***
F
Sensitivity
1−Specificity
AUC at 1 years: 0.895
AUC at 3 years: 0.834
AUC at 5 years: 0.862
G
Sensitivity
1−Specificity
AUC at 1 years: 0.719
AUC at 3 years: 0.714
AUC at 5 years: 0.698
H
Strata risk=high risk=low
Survival probability
p < 0.0001
Time
Number at risk
risk=high 42 18 7 1 0
risk=low 43 27 11 5 0
I
Survival time (years)
Dead
Alive
Risk score
high risk
low risk
J
type
SCD
MYC
EPYC
AOC3
KLK2
matrix_18 type
high
low

Figure 4 Identification of characteristic genes and construction of prognostic models. (A) The Venn diagram represents the intersection of the OSA-DEGs gene set and the group-DEGs gene set, with the number of intersecting genes being 274. (B) The results of the univariate regression analysis displayed genes with a significance level less than 0.05. (C) The LASSO regression coefficient path plot shows each line representing a variable, with the vertical axis indicating coefficient values and the horizontal axis representing Log(λ) values. (D) The cross-validation curve of the LASSO regression shows that a smaller value on the vertical axis indicates better fitting performance. (E) The results of the multivariate regression analysis ultimately identified 5 characteristic genes. (F) The ROC analysis results for the training set indicate AUC values of 0.895, 0.834, and 0.862 at 1, 3, and 5 years, respectively. (G) The AUC values of the ROC curve for the validation set are 0.719, 0.714, and 0.698 at 1, 3, and 5 years, respectively. (H) The K-M curve reveals that the survival outcomes of the low-risk group are more favorable than those of the high-risk group. (I) The findings showing the distribution of survival status and risk scores for the high-risk and low-risk groups. (J) The heatmap shows the expression levels of characteristic genes in the two risk groups.

3.5 Constructing a nomogram for independent prognostic analysis

Survival analysis of the feature genes revealed that while EPYC showed a survival trend, the difference was not statistically significant (P=0.05384, Figure 5A). In contrast, MYC exhibited a significant difference between risk groups (Figure 5B). We then performed univariate and multivariate regression analyses integrating clinical features and risk scores, identifying M stage and risk score as independent prognostic factors (P<0.05, Figure 5C-D). To facilitate clinical application, we developed a nomogram integrating risk score and clinical variables to predict 1-, 3-, and 5-year survival (Figure 5E). Calibration curves (Figure 5F) showed that the nomogram's predicted outcomes closely matched observed survival in the training set. Similar results were observed in the validation set (Figure 5G). Decision curve analysis (DCA) further demonstrated that the nomogram provided considerable net clinical benefit for predicting survival at 1, 3, and 5 years (Figure 5H). In summary, our findings suggest that the nomogram exhibits strong predictive power, and the 5-gene-based model may serve as a robust independent prognostic indicator for OSA.

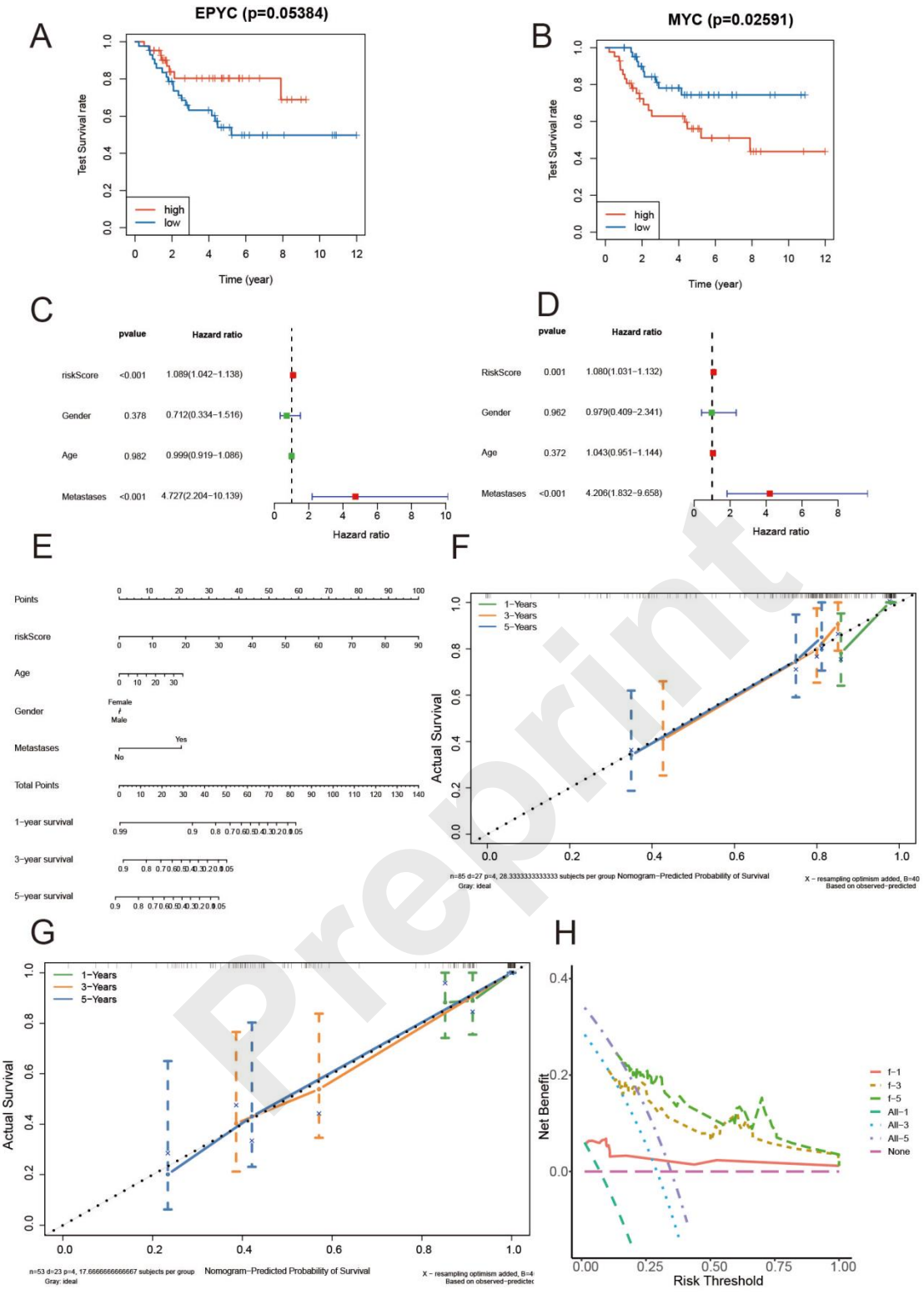

Figure 5 Development and assessment of nomograms. (A) The findings of K-M curve for EPYC. (B) The K-M curve illustrates a markedly greater survival rate for MYC in the low-risk category compared to the high-risk category, P =0.02591. (C) Outcomes of univariate regression analyses utilizing risk scores and clinical data. (D) The findings of multivariate regression analyses based on risk score and clinical information. (E) A nomogram for comprehensively assessing the prognostic performance of OSA. (F) Calibration curves for year 1, year 3, and year 5 in the

training dataset. (G) Verification of centralized calibration curve findings, the horizontal coordinate represents the predicted probability and the vertical coordinate represents the actual probability of occurrence. (H) The findings from the DCA curve analysis over periods of 1, 3, and 5 years reveal that the horizontal axis illustrates the threshold probability, whereas the vertical axis reflects the net benefits achieved.

3.6 Examination of the immune environment between high-risk and low-risk groups

To comprehensively assess immune infiltration and prognosis across risk groups, ssGSEA was used to compare immune-related functions and cell infiltration between high- and low-risk groups. As shown in Figure 6A, immune infiltration was markedly higher in the low-risk group. Figure 6B confirms this with box plots demonstrating elevated infiltration levels for most immune cell types. Consistently, the low-risk group showed significantly higher ESTIMATE, immune, and stromal scores, while tumor purity was increased in the high-risk group (Figure 6C). Metastasis rates were also lower in the low-risk group (Figure 6D).

Immune checkpoint gene expression was broadly upregulated in the low-risk group (Figure 6E). Correlation analysis revealed that AOC3 and EPYC were positively associated with B cells, while MYC showed a negative correlation. Similarly, AOC3 and KLK2 positively correlated with pDCs, whereas MYC was negatively correlated. AOC3 (Figure 6F), KLK2 (Figure 6G), and EPYC (Figure 6H) were positively linked to most immune cells, while MYC (Figure 6I) and SCD1 (Figure 6J) showed negative correlations.

To investigate interactions with oncogenic pathways, we analyzed the expression correlation between canonical oncogenes and signature genes in the TARGET-OS cohort. As shown in Supplementary Figure 1, KLK2 was negatively correlated with FAS ($r = -0.41$, $P<0.01$), and SCD1 positively correlated with NRAS ($r = 0.32$, $P<0.01$), suggesting possible crosstalk between CMRG-derived markers and oncogenic signaling in osteosarcoma.

We further evaluated the association between the risk score and the tumor immune cycle. As illustrated in Figure 6K, the risk score and most characteristic genes were negatively correlated with step 4 (immune cell recruitment). Additionally, Figure 6L shows that infiltration scores for immune and tissue repair cells were significantly higher in the low-risk group.

Overall, these findings indicate a more active immune microenvironment in low-risk patients, who may therefore benefit more from immunotherapy.

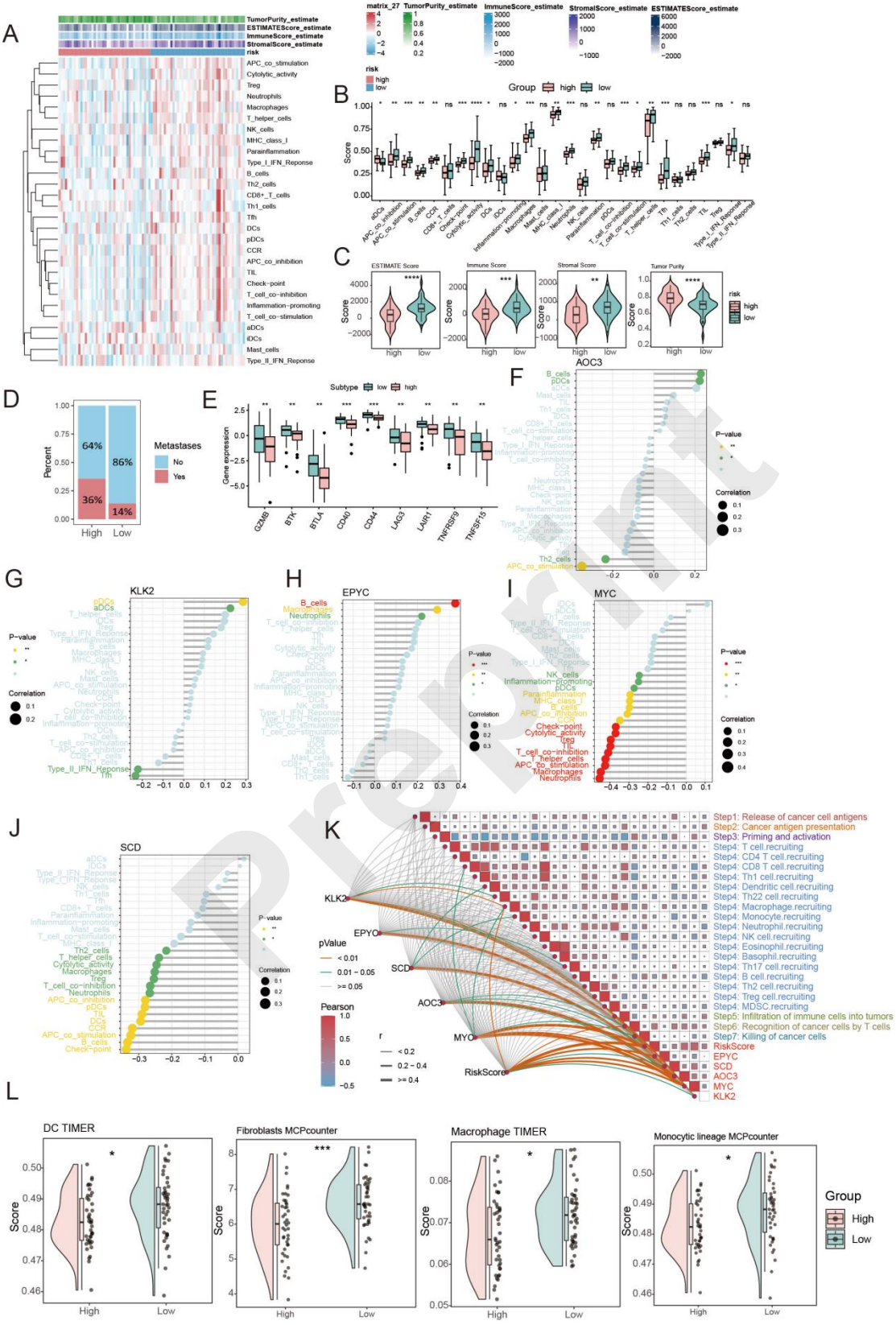

Figure 6 Evaluation of immune activity and infiltration of immune cells across the two risk categories. (A) The heatmap displays variations in immune cell infiltration between the two risk

groups. (B) The box plots illustrate variations in immune cell infiltration expression between the two risk groups. (C) The violin plot illustrates the variation in multiple scores across the two risk groups. (D) Comparison of disease metastasis between high and low risk groups. (E) Comparison of immune checkpoint gene expression in high-risk versus low-risk groups. Correlation analysis diagram of characteristic genes AOC3 (F), KLK2 (G), EPYC (H), MYC (I), and SCD1 (J) with immune cell infiltration. (K) Heatmap of the association between signature genes, risk scores, and the immunization cycle. (L) Infiltration levels for various cell types, such as dendritic cells (DC), fibroblasts, macrophages, and cells from the monocytic lineage, were compared between high-risk and low-risk groups. ns denotes no significant difference, * signifies $P<0.05$, ** represents $P<0.01$, and *** indicates $P<0.001$.

3.7 Response to PD-L1 inhibition immunotherapy according to risk scores

Following the assessment of immune infiltration, we extracted data from the IMvigor210 cohort regarding responses to PD-L1 inhibitor immunotherapy from public databases. In this cohort of 348 patients, responses to PD-L1 blockade varied and included stable disease (SD), partial response (PR), complete response (CR), and disease progression (PD). Our analysis utilizing K-M curves demonstrated that the survival outcomes for the low-risk group were significantly better than those of the high-risk group (Figure 7A). Importantly, we classified SD and PD as NR (Not Responding) and CR and PR as R (Responding). The analysis indicated that patients in the R group exhibited significantly lower risk scores compared to those in the NR group (Figure 7B). Additionally, the proportion of NR patients in the low-risk group was significantly lower than that in the high-risk group (Figure 7C).

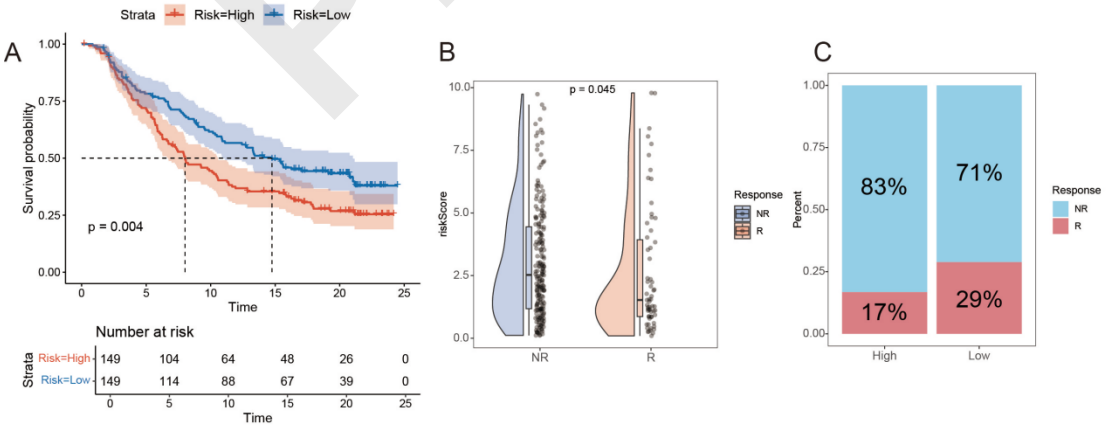

Figure 7 Evaluating immune therapy effectiveness using risk scores from public databases. (A) Comparison of survival analysis differences among subgroups in the IMvigor210 cohort. (B) Variations in immunotherapy effectiveness according to risk assessments. (C) Proportion of various immunotherapy reactions categorized by risk groups.

3.8 Functional enhancement of differentially expressed genes in high and low-risk cohorts

To further investigate the biological functions and underlying molecular mechanisms across risk groups, we conducted differential expression analysis between the high- and low-risk groups (|logFC|>1, P<0.05, Figure 8A). This analysis identified 908 upregulated and 413 downregulated genes, which were subsequently subjected to GO and KEGG enrichment analyses. GO analysis revealed that differentially expressed genes were significantly enriched in cell membrane structure-related pathways within the Biological Process (BP) category (Figure 8B), protein metabolism pathways within the Molecular Function (MF) category (Figure 8C), and neuroregulation-related pathways within the Cellular Component (CC) category (Figure 8D). Additionally, KEGG analysis indicated that upregulated genes were enriched in neuroregulation and protein metabolism pathways (Figure 8E), whereas downregulated genes were associated with immune regulation-related pathways (Figure 8F).

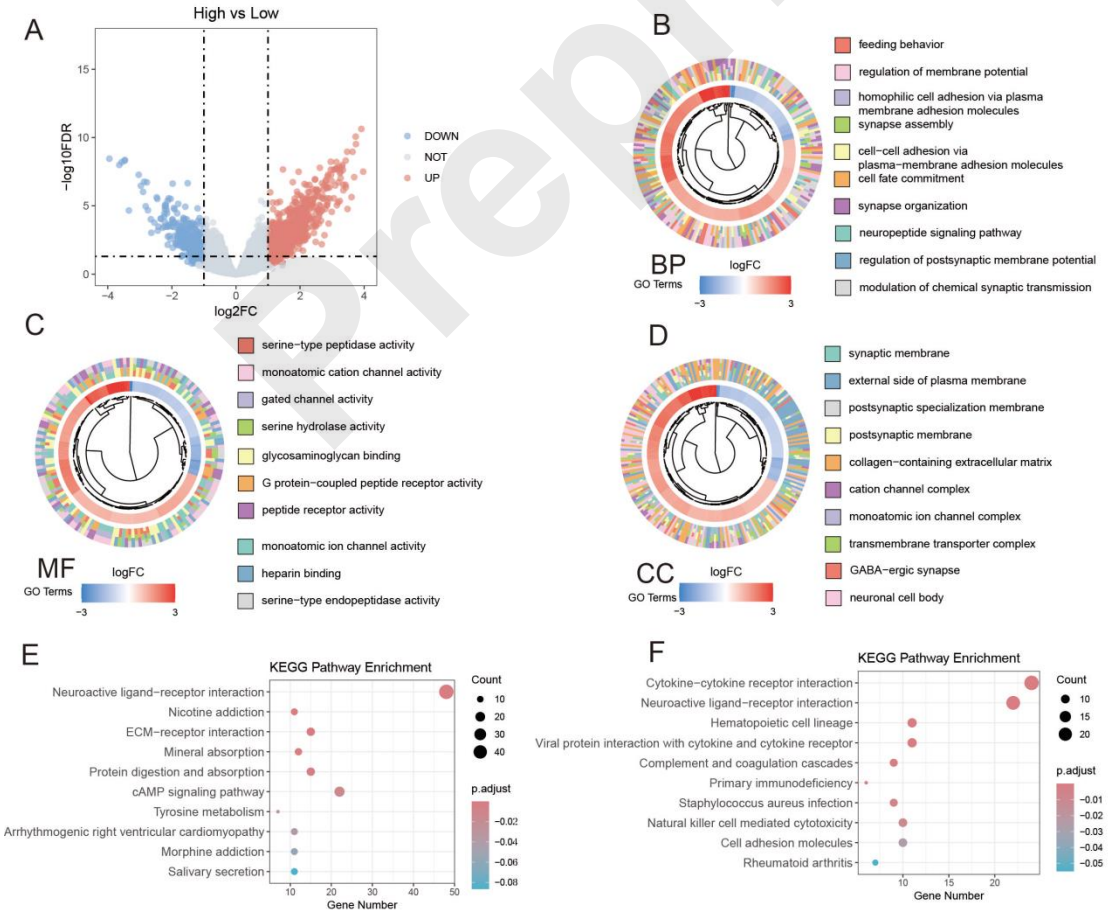

Figure 8 Investigation of biological roles and pathway activities in high and low-risk groups.

(A) Volcano map illustrating genes expressed differently between high and low-risk groups. Functional Analysis in (B) Biological Activities (BP), (C) Molecular Roles (MF), and (D) Cellular Structures (CC). (E) KEGG enrichment assessment of increased gene expression. (F) KEGG enrichment assessment of downregulated genes.

3.9 Analysis of the relationship between TME and risk score-related cell types based on single-cell sequencing

To investigate the relationship between the TME and cell types associated with risk scores, we analyzed single-cell sequencing data from 11 OSA patients in the GSE152048 dataset. After quality control and batch effect removal, we clustered and annotated the filtered cells into nine major cell types: macrophages, chondroblastic cells, osteoclasts, T cells, cycling cells, monocytes, osteoblastic cells, pericytes, endothelial cells, NK cells, and mast cells (Figure 9A). Utilizing the SCISSOR algorithm alongside sequencing data from TARGET-OS patients and risk group information, we identified cell types correlated with different risk levels (Figure 9B), [25]. Consistent with expectations, we observed more high-risk-associated cell types in patients with recurrence and metastasis (Figure 9C).

We then employed CellChat to infer overall intercellular communication based on ligand-receptor signaling. As illustrated in Figure 9D, the results depict the number of cells involved in interactions, while Figure 9E shows the frequency of interactions among different cell types. Collectively, theses findings indicate significant cell-cell communication, which is essential for understanding immune cell functions within the TME. Furthermore, Transforming Growth Factor Beta (TGFb, Figure 9F) and Mitogen-Activated Protein Kinase Kinase Kinase (MKK, Figure 9G) signaling pathways were implicated in cell proliferation, differentiation, and immune regulation, playing multifaceted roles in tumor progression. We further analyzed the relationships between the identified cell types and these pathways, and found distinct intercellular communication patterns targeting these pathways. Additionally, we assessed the distribution of characteristic genes across immune cell types and observed that MYC and SCD1 had superior cell-type-specific expression compared to other genes (Supplementary Figure 2).

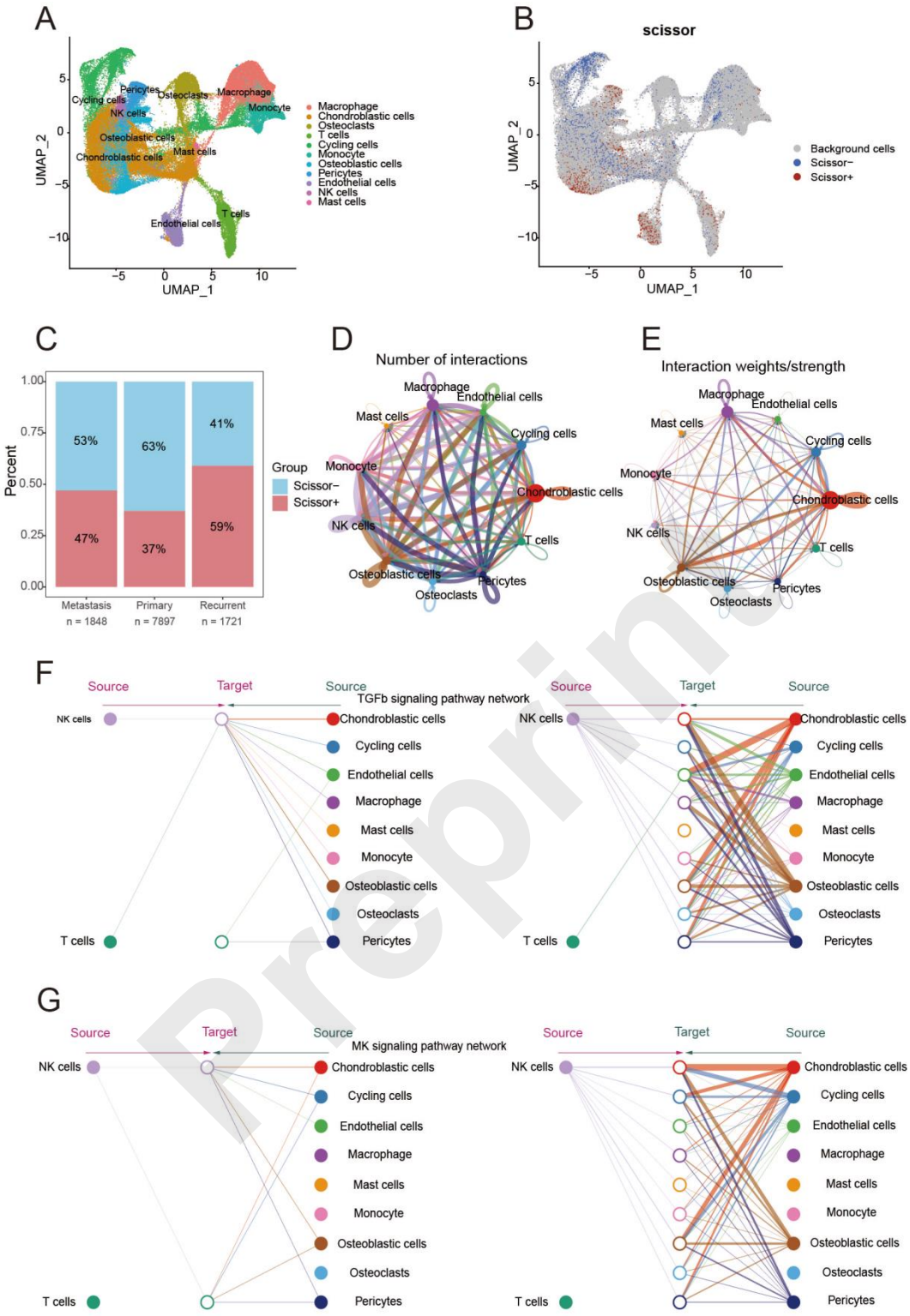

487

488 Figure 9 Single-cell sequencing evaluation of various cells in the TME according to risk
489 scores. (A) UMAP examines 9 cellular clusters in samples from OSA patients. (B) UMAP
490 visualization of cell distribution according to risk scores. (C) The bar chart illustrates the
491 distribution percentage of various cells in the sample species according to their risk score. (D) The

quantity of cells that are engaged in communication and interaction with one another is depicted here. Different colored circles represent the cell count, with larger circles signifying a higher number of cells involved. (E) Intensity of intercellular communication exchanges: the thicker the line, the greater the intensity. (F) Examination of cell interactions in the TGFb (F) and MKK signaling pathway (G).

3.10 Comprehensive analysis of potential anti-OSA drugs

This study employed the CellMiner database to predict the correlation between feature genes and drug sensitivity, identifying a significant positive relationship between MYC and DMAPT (Figure 10A), Obatoclax (Figure 10B), 8-Chloro-adenosine (Figure 10C), and Palbociclib (Figure 10D). We also conducted a statistical analysis of approved drugs targeting feature genes, providing theoretical support for selecting suitable therapeutic agents for OSA patients (Figure 10E). Notably, our analysis of drug sensitivity between risk groups showed that patients in the low-risk group had significantly lower IC50 values for Cisplatin (Figure 10F) and Temozolomide (Figure 10G), indicating that these drugs may be more effective in low-risk patients.

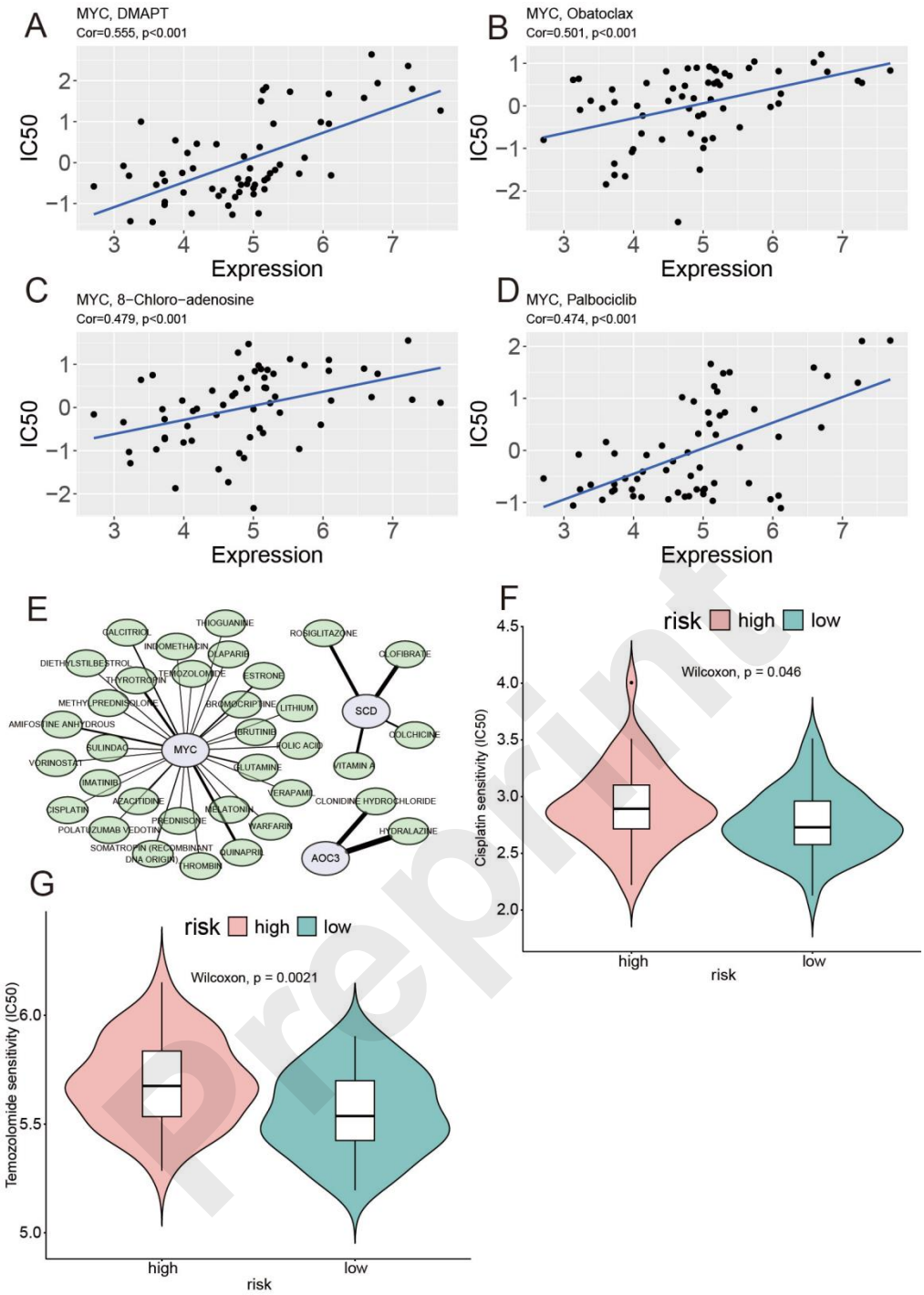

Figure 10 Comprehensive analysis of potential anti-tumor drugs. Significance Analysis of Characterized Genes MYC with DMAPT (A), Obatoclax (B), 8-Chloro-adenosine (C) and Palbociclib (D), $P<0.001$. (E) The network diagram illustrates the data on feature genes associated with known interacting drugs. Violin plot representation of drug sensitivity analysis between high

and low risk groups including Cisplatin (F) and Temozolomide (G).

3.11 Comprehensive experimental analysis of characteristic gene expression, cell apoptosis, and cytotoxicity

Next, we validated the expression levels of the characteristic genes in the osteoblastic cell line hFOB1.19 and the OSA cell line U2OS. The qRT-PCR results (Figure 11A) showed that EPYC was significantly overexpressed in U2OS cells. Similarly, SCD1 and AOC3 were also significantly upregulated in OSA cells. In contrast, no significant differences were observed in the expression of MYC and KLK2. These findings further confirm the differential expression of characteristic genes between normal and OSA cells. The MTT cytotoxicity assay results (Figure 11B) demonstrated that both Temozolomide and Cisplatin exhibited concentration dependent enhanced inhibitory effects on the proliferation of OSA cell lines U2OS and SAOS2. SAOS2 cells showed higher sensitivity to both drugs, with a significantly lower IC50 (81.52 μM) for Temozolomide compared to U2OS cells (112.4 μM), and a markedly lower IC50 (4.087 μM) for Cisplatin (9.314 μM). TUNEL apoptosis assays further corroborated the heightened sensitivity of SAOS2 cells, revealing a significantly higher proportion of TUNEL positive cells in SAOS2 cells following treatment with either Temozolomide or Cisplatin, compared to U2OS cells (Figure 11C-D). Collectively, these data consistently demonstrate that SAOS2 cells possess higher sensitivity than U2OS cells to Temozolomide and Cisplatin induced cytotoxicity and apoptosis.

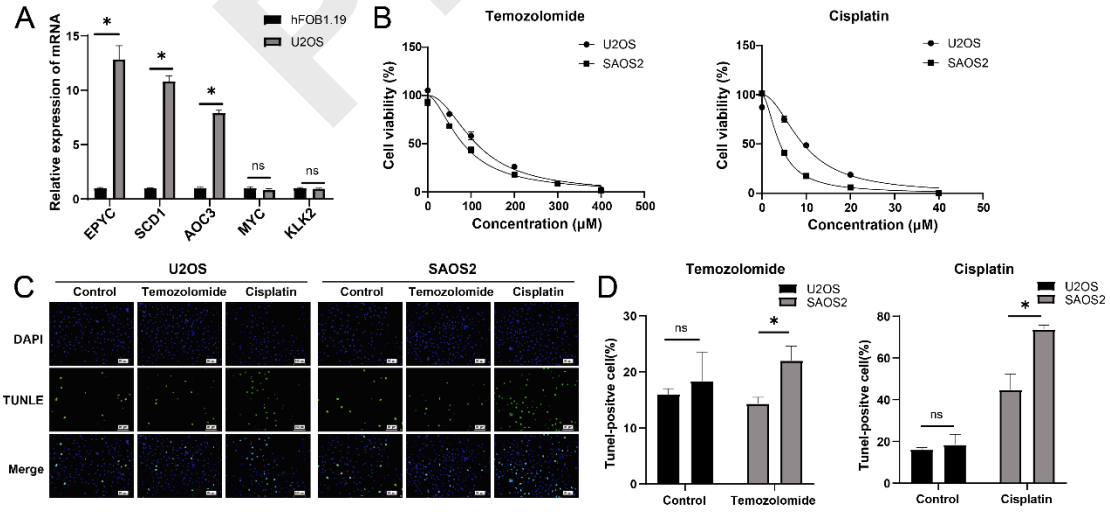

Figure 11 Comprehensive experimental analysis of characteristic gene expression, cell apoptosis, and cytotoxicity. (A) qRT-PCR Results of EPYC, SCD1, and AOC3 in Normal Cells

and OSA Cells. (B) MTT assay to detect the viability of U2OS and SAOS2 cells treated with different concentrations of temozolomide or cisplatin for 48 hours. (C) Representative images of TUNEL assay for cell apoptosis. (D) Quantitative analysis results of TUNEL assay for cell apoptosis. ns denotes no significant difference, * signifies $P<0.05$.

4.Discussion

Immunotherapy plays a crucial role in tumor treatment. Although it has not yet been approved for OSA, several approaches — including immune checkpoint inhibitors, bispecific antibodies, and chimeric antigen receptor (CAR) T cells—are actively undergoing clinical development [26]. Consequently, research on immunotherapy for OSA is expected to become a key focus in the field. CMRGs are essential for regulating T cell activity, maintaining immune balance, and modulating immune responses [27, 28]. This study evaluated the prognostic survival outcomes of OSA patients based on CMRGs, and identified five characteristic genes: EPYC, SCD1, AOC3, MYC, and KLK2.

Epiphycan (EPYC), located on human chromosome 12, is a protein-coding gene composed of seven exons [29]. Its primary function is to regulate fibril formation through interactions with collagen fibrils and other extracellular matrix proteins [30]. EPYC has been implicated in various diseases. Liang et al. demonstrated that EPYC serves as a diagnostic marker for osteoarthritis, supported by both machine learning and in vitro experiments [31]. Similarly, Zhang et al. confirmed EPYC as a characteristic gene for osteoarthritis and reported a significant correlation between EPYC expression and immune infiltration [32]. In addition, EPYC has been identified as a prognostic biomarker for pancreatic cancer [30]. Our experimental results revealed that EPYC is highly expressed in OSA tissues, and that patients in the low-risk group exhibited significantly better survival outcomes. Furthermore, EPYC expression was positively correlated with immune cell infiltration, suggesting its potential as a prognostic biomarker for OSA.

Stearoyl-CoA desaturase 1 (SCD1) is an enzyme located in the endoplasmic reticulum, synthesized from saturated fatty acid (SFA) precursors [33]. A review study reported that SCD1 acts as an autophagy inducer, affecting cancer cell proliferation and metastasis [34]. In colorectal cancer, SCD1 plays a key role in drug-induced growth inhibition, and SCD1 knockout enhances sensitivity to ferroptosis [35].

Notably, Cai et al. found that SCD1 regulates the Akt/mTOR pathway, promoting lipid metabolism and enhancing OSA cell proliferation [36].

Amine oxidase copper containing 3 (AOC3) encodes cell adhesion proteins that are involved in lymphocyte extravasation and recirculation [37]. Dysregulation of AOC3 expression has been shown to influence cancer progression. Studies report that AOC3 expression is decreased in colorectal cancer tissues and serum, with low levels correlating with poor prognosis [38, 39]. Conversely, high AOC3 expression in thymic carcinoma has been significantly associated with unfavorable prognosis [40].

MYC is a transcription factor and a key driver of human tumorigenesis. The MYC protein mainly regulates transcriptional processes, including elongation, DNA replication, and cell cycle progression [41, 42]. Targeting MYC has emerged as an effective strategy for cancer therapy [43, 44].

Human kallikrein 2 (KLK2) belongs to the kallikrein gene family and functions as a serine protease [45, 46]. Recent studies suggest that KLK2 may be a therapeutic target in prostate cancer, where elevated KLK2 expression correlates with increased proliferation and reduced apoptosis [47]. KLK2 has also been established as a prognostic biomarker for prostate cancer [48]. Our study is the first to employ KLK2 in a prognostic model for OSA, demonstrating its value in accurately predicting survival.

In conclusion, this study identifies five characteristic genes based on CMRGs to construct a prognostic model, aiming to support personalized treatment strategies for OSA patients and enhance the precision of clinical decision-making.

Most immunotherapy strategies rely on the patient's intrinsic immune response, typically progressing through three stages: immune surveillance, self-regulation, and immune evasion [14]. Immune checkpoint inhibitors are central to these mechanisms and have shown promise in treating OSA [14, 49]. CTLA-4 binds to B7 on Tregs and cancer cells, thereby suppressing T cell activity. Blocking this interaction can restore T cell functionality [49]. Notably, anti-PD-1 therapy in an OSA mouse model led to increased expression of GZMB in T cells [50, 51]. Yoshida et al. reported a positive correlation between GZMB and IFN-γ expression, with elevated GZMB levels linked to improved survival in OSA patients [52]. These findings underscore the importance of GZMB in immunotherapy efficacy. Our analysis revealed elevated GZMB expression in the low-risk group, along with other immune checkpoint-related genes such as BTK, BTLA, CD40, CD44, LAG3, LAIR1, TNFRSF9, and TNFSF15,

suggesting that low-risk patients may benefit more from immunotherapy.

Dimethylaminoparthenolide (DMAPT) is an anti-inflammatory compound that inhibits prostate cancer [53] and bladder cancer progression [54]. Obatoclax, a BCL2 family inhibitor, induces thyroid cancer cell death by disrupting lysosomal function [55]. 8-chloro-adenosine is a nucleoside analog long used in leukemia research [56]. Palbociclib is an orally available CDK4/6 inhibitor, which suppresses proliferation and induces cell cycle arrest, with broad application in breast cancer therapy [57, 58]. Our study uncovered a significant positive correlation between MYC expression and the IC50 values of these drugs. Moreover, our analysis revealed that low-risk patients are more sensitive to Cisplatin and Temozolomide, supporting their clinical utility in this subgroup.

Our correlation analysis (Supplementary Figure 1) revealed intriguing associations between the CMRG-based signature and classic oncogenes. The negative correlation between KLK2 and FAS suggests that KLK2 may suppress FAS-mediated apoptosis, a mechanism known to contribute to chemotherapy resistance [59]. Conversely, the positive correlation between SCD1 and NRAS supports NRAS's role in activating SREBP-1c-driven lipogenesis—a pathway that increases the production of monounsaturated fatty acids (MUFA) through SCD1-mediated desaturation, thereby enhancing membrane fluidity, oncogenic signaling, and tumor cell proliferation [60, 61]. Notably, the absence of correlation with TP53—a gene frequently mutated in OSA—indicates that our CMRG signature reflects biological pathways distinct from canonical tumor suppressor mechanisms.

This first comprehensive study to construct a CMRG-based prognostic model for OSA integrates subtype classification, immune profiling, drug sensitivity prediction, and experimental validation, thereby expanding the understanding of immune regulation in OSA and proposing novel clinical biomarkers. However, several limitations warrant consideration: the analyses primarily rely on public databases, which may introduce population bias; although qRT-PCR validated gene expression, further in vivo and clinical studies are needed to confirm functional roles; and the risk model's generalizability requires external validation due to the lack of prospective cohorts.

5.Conclusion

This study subdivided OSA samples into three subtypes based on CMRGs and analyzed the differences in immune cell infiltration levels among the subtypes, revealing that subtype 3 exhibited significantly higher immune infiltration levels than subtypes 1 and 2. By merging subtypes 2 and 3, we identified differentially expressed genes, ultimately selecting five characteristic genes through LASSO and multivariable regression analysis to construct a prognostic model for OSA. Our results elucidate that the low-risk group has better prognostic outcomes, suggesting that patients in this group may benefit more from immunotherapy. Additionally, single-cell sequencing results comprehensively characterized the distribution of immune cells and the expression levels of characteristic genes within these cells. In summary, the prognostic prediction model developed in this study significantly aids in formulating effective strategies to enhance survival rates in OSA patients, providing a theoretical basis for personalized treatment approaches.

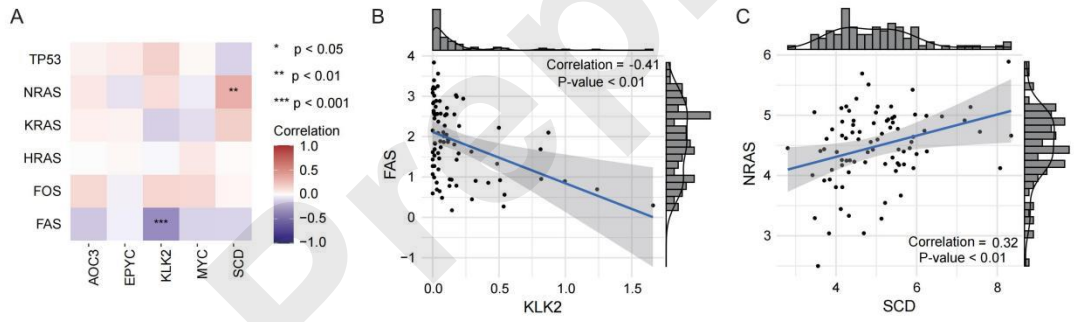

Supplementary Figure 1 Correlation between characteristic genes and canonical oncogenes in TARGET-OS cohort (A) Heatmap of correlation between canonical oncogenes and characteristic genes. (B) Scatter plot of correlation between FAS and KLK2. (C) Scatter plot of correlation between NRAS and SCD.

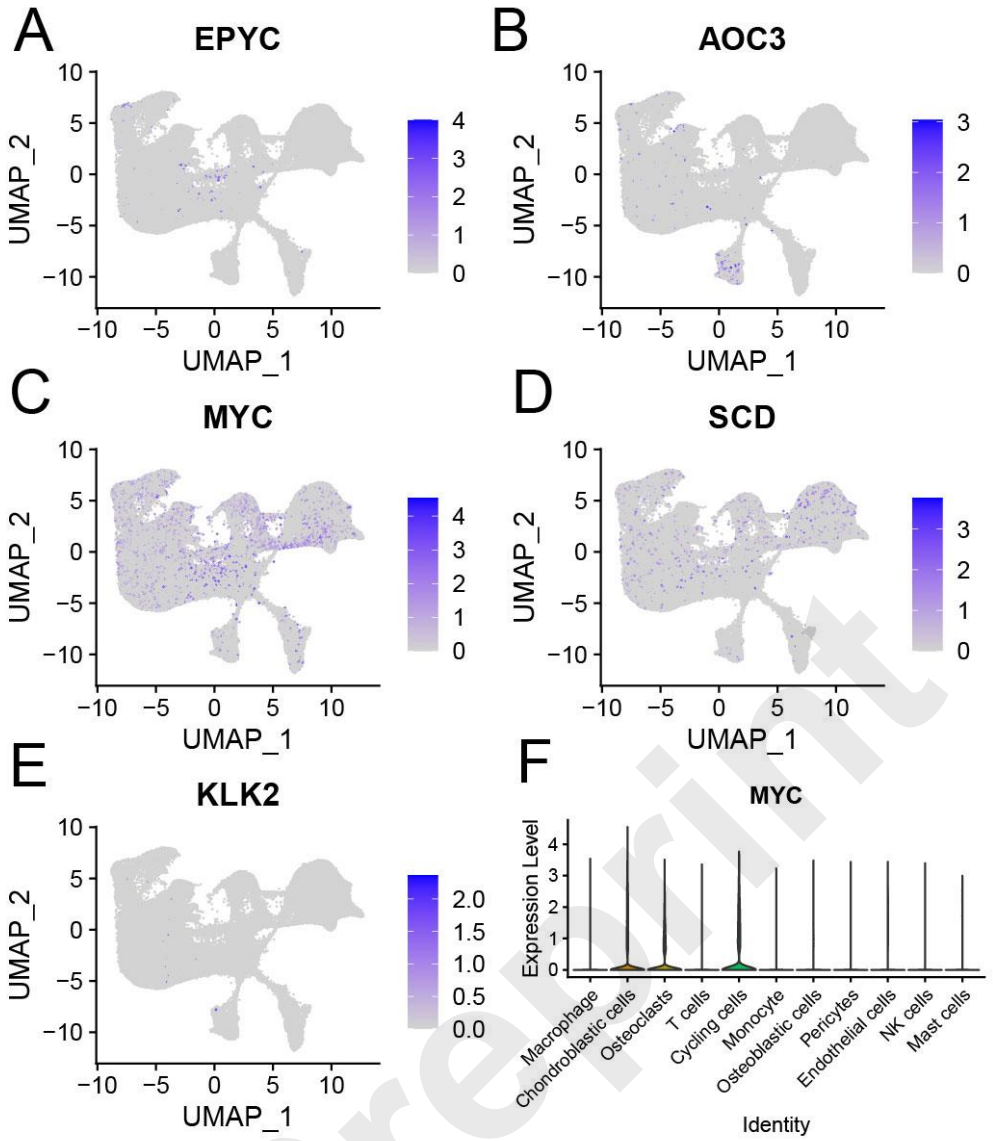

664

665 Supplementary Figure 2 The distribution of characteristic genes in cells. The distribution of
666 the characteristic gene EPYC (A), AOC3 (B), MYC (C), SCD1 (D) and KLK2 (E) in various
667 immune cells. The expression levels of MYC (F) in immune cells.

668 Supplementary Table S1: CMRGs genelist

669 Supplementary Table S2: DECMRGs genelist

670 Supplementary Table S3: group-DEGs genelist

671 Supplementary Table S4: IMvigor210 samples

672

673

References

[1] Arndt C A,P S Rose,A L Folpe et al. Common musculoskeletal tumors of childhood and adolescence. *Mayo Clin Proc* 2012;87: 475-87.

[2] Huang X,J Zhao,J Bai et al. Risk and clinicopathological features of osteosarcoma metastasis to the lung: A population-based study. *J Bone Oncol* 2019;16: 100230.

[3] Eaton B R,R Schwarz,R Vatner et al. Osteosarcoma. *Pediatr Blood Cancer* 2021;68 Suppl 2: e28352.

[4] Gianferante D M,L Mirabello, S A Savage. Germline and somatic genetics of osteosarcoma - connecting aetiology, biology and therapy. *Nat Rev Endocrinol* 2017;13: 480-491.

[5] Li J,X Tang,Y Du et al. Establishment of an Autophagy-Related Clinical Prognosis Model for Predicting the Overall Survival of Osteosarcoma. *Biomed Res Int* 2021;2021: 5428425.

[6] Meltzer P S, L J Helman. New Horizons in the Treatment of Osteosarcoma. *N Engl J Med* 2021;385: 2066-2076.

[7] Jamal-Hanjani M,S A Quezada,J Larkin et al. Translational implications of tumor heterogeneity. *Clin Cancer Res* 2015;21: 1258-66.

[8] Wu C,S Gong,Y Duan et al. A tumor microenvironment-based prognostic index for osteosarcoma. *J Biomed Sci* 2023;30: 23.

[9] Momen M,N L Kohler,E E Binversie et al. Heritability and genetic variance estimation of Osteosarcoma (OSA) in Irish Wolfhound, using deep pedigree information. *Canine Med Genet* 2021;8: 9.

[10] Wei X,J Feng,L Chen et al. METTL3-mediated m6A modification of LINC00520 confers glycolysis and chemoresistance in osteosarcoma via suppressing ubiquitination of ENO1. *Cancer Lett* 2024: 217194.

[11] Jiang M,Y Jike,K Liu et al. Exosome-mediated miR-144-3p promotes ferroptosis to inhibit osteosarcoma proliferation, migration, and invasion through regulating ZEB1. *Mol Cancer* 2023;22: 113.

[12] Xiangyang Cheng C B, Yiming Zhang, Huijie Gu, Guangnan Chen, Liang Wu APOE suppresses osteosarcoma by modulating ferroptosis through the mTOR/Stat3 signaling pathway. *Archives of Medical Science* 2025.

[13] Bilotta M T,A Antignani, D J Fitzgerald. Managing the TME to improve the efficacy of cancer therapy. *Front Immunol* 2022;13: 954992.

[14] Chen C,L Xie,T Ren et al. Immunotherapy for osteosarcoma: Fundamental mechanism, rationale, and recent breakthroughs. *Cancer Lett* 2021;500: 1-10.

[15] Singh S,D Hassan,H M Aldawsari et al. Immune checkpoint inhibitors: a promising anticancer therapy. *Drug Discov Today* 2020;25: 223-229.

[16] Sanmamed M F, L Chen. A Paradigm Shift in Cancer Immunotherapy: From Enhancement to Normalization. *Cell* 2018;175: 313-326.

[17] Capece D,D Verzella,M Fischietti et al. Targeting costimulatory molecules to improve antitumor immunity. *J Biomed Biotechnol* 2012;2012: 926321.

[18] Fan M K,L L Qi,Q Zhang et al. The Updated Status and Future Direction of Immunotherapy Targeting B7-H1/PD-1 in Osteosarcoma. *Cancer Manag Res* 2021;13: 757-764.

[19] Zhang C,Z Zhang,F Li et al. Large-scale analysis reveals the specific clinical and immune features of B7-H3 in glioma. *Oncoimmunology* 2018;7: e1461304.

[20] Janakiram M,J M Chinai,A Zhao et al. HHLA2 and TMIGD2: new immunotherapeutic targets of the B7 and CD28 families. *Oncoimmunology* 2015;4: e1026534.

[21] Ward-Kavanagh L K,W W Lin,J R Šedý et al. The TNF Receptor Superfamily in Co-stimulating and Co-inhibitory Responses. *Immunity* 2016;44: 1005-19.
[22] Zhang C,Z Zhang,N Sun et al. Identification of a costimulatory molecule-based signature for predicting prognosis risk and immunotherapy response in patients with lung adenocarcinoma. *Oncoimmunology* 2020;9: 1824641.
[23] Li H,S Liu,C Li et al. TNF Family-Based Signature Predicts Prognosis, Tumor Microenvironment, and Molecular Subtypes in Bladder Carcinoma. *Front Cell Dev Biol* 2021;9: 800967.
[24] Ren Q,P Zhang,H Lin et al. A novel signature predicts prognosis and immunotherapy in lung adenocarcinoma based on cancer-associated fibroblasts. *Front Immunol* 2023;14: 1201573.
[25] Sun D,X Guan,A E Moran et al. Identifying phenotype-associated subpopulations by integrating bulk and single-cell sequencing data. *Nat Biotechnol* 2022;40: 527-538.
[26] Yu S, X Yao. Advances on immunotherapy for osteosarcoma. *Mol Cancer* 2024;23: 192.
[27] Bäck M,C Weber, E Lutgens. Regulation of atherosclerotic plaque inflammation. *J Intern Med* 2015;278: 462-82.
[28] Zhao Y,Q Zheng, L Jin. The Role of B7 Family Molecules in Maternal-Fetal Immunity. *Front Immunol* 2020;11: 458.
[29] Hanada Y,Y Nakamura,Y Ishida et al. Epiphycan is specifically expressed in cochlear supporting cells and is necessary for normal hearing. *Biochem Biophys Res Commun* 2017;492: 379-385.
[30] Yang Z,H Li,J Hao et al. EPYC functions as a novel prognostic biomarker for pancreatic cancer. *Sci Rep* 2024;14: 719.
[31] Liang Y,F Lin, Y Huang. Identification of Biomarkers Associated with Diagnosis of Osteoarthritis Patients Based on Bioinformatics and Machine Learning. *J Immunol Res* 2022;2022: 5600190.
[32] Zhang J,S Zhang,Y Zhou et al. KLF9 and EPYC acting as feature genes for osteoarthritis and their association with immune infiltration. *J Orthop Surg Res* 2022;17: 365.
[33] Paton C M, J M Ntambi. Biochemical and physiological function of stearoyl-CoA desaturase. *Am J Physiol Endocrinol Metab* 2009;297: E28-37.
[34] Ascenzi F,C De Vitis,M Maugeri-Saccà et al. SCD1, autophagy and cancer: implications for therapy. *J Exp Clin Cancer Res* 2021;40: 265.
[35] Chen H,Q Qi,N Wu et al. Aspirin promotes RSL3-induced ferroptosis by suppressing mTOR/SREBP-1/SCD1-mediated lipogenesis in PIK3CA-mutant colorectal cancer. *Redox Biol* 2022;55: 102426.
[36] Cai F,L Liu,Y Bo et al. LncRNA RPARP-AS1 promotes the progression of osteosarcoma cells through regulating lipid metabolism. *BMC Cancer* 2024;24: 166.
[37] Boyer D S,J F Rippmann,M S Ehrlich et al. Amine oxidase copper-containing 3 (AOC3) inhibition: a potential novel target for the management of diabetic retinopathy. *Int J Retina Vitreous* 2021;7: 30.
[38] Ahmad Zawawi S S,N A S Mohd Azram,S Sulong et al. Identification of AOC3 and LRRC17 as Colonic Fibroblast Activation Markers and Their Potential Roles in Colorectal Cancer Progression. *Asian Pac J Cancer Prev* 2023;24: 3099-3107.
[39] Ward S T,C J Weston,E L Shepherd et al. Evaluation of serum and tissue levels of VAP-1 in colorectal cancer. *BMC Cancer* 2016;16: 154.
[40] Lai Y C,S J Chang,J Kostoro et al. Vascular adhesion protein-1 as indicator of breast cancer tumor aggressiveness and invasiveness. *Apmis* 2018;126: 755-761.
[41] Lourenco C,D Resetca,C Redel et al. MYC protein interactors in gene transcription and cancer. *Nat Rev Cancer* 2021;21: 579-591.

[42] Baluapuri A,E Wolf, M Eilers. Target gene-independent functions of MYC oncoproteins. *Nat Rev Mol Cell Biol* 2020;21: 255-267.
[43] Duffy M J,S O'Grady,M Tang et al. MYC as a target for cancer treatment. *Cancer Treat Rev* 2021;94: 102154.
[44] Chen H,H Liu, G Qing. Targeting oncogenic Myc as a strategy for cancer treatment. *Signal Transduct Target Ther* 2018;3: 5.
[45] Avgeris M,K Mavridis, A Scorilas. Kallikrein-related peptidase genes as promising biomarkers for prognosis and monitoring of human malignancies. *Biol Chem* 2010;391: 505-11.
[46] Paniagua-Herranz L,I Moreno,C Nieto-Jiménez et al. Genomic and Immunologic Correlates in Prostate Cancer with High Expression of KLK2. *Int J Mol Sci* 2024;25.
[47] Shang Z,Y Niu,Q Cai et al. Human kallikrein 2 (KLK2) promotes prostate cancer cell growth via function as a modulator to promote the ARA70-enhanced androgen receptor transactivation. *Tumour Biol* 2014;35: 1881-90.
[48] Kohli M,P G Rothberg,C Feng et al. Exploratory study of a KLK2 polymorphism as a prognostic marker in prostate cancer. *Cancer Biomark* 2010;7: 101-8.
[49] Zhang Z,X Tan,Z Jiang et al. Immune checkpoint inhibitors in osteosarcoma: A hopeful and challenging future. *Front Pharmacol* 2022;13: 1031527.
[50] Zheng B,T Ren,Y Huang et al. PD-1 axis expression in musculoskeletal tumors and antitumor effect of nivolumab in osteosarcoma model of humanized mouse. *J Hematol Oncol* 2018;11: 16.
[51] Ratti C,L Botti,V Cancila et al. Trabectedin Overrides Osteosarcoma Differentiative Block and Reprograms the Tumor Immune Environment Enabling Effective Combination with Immune Checkpoint Inhibitors. *Clin Cancer Res* 2017;23: 5149-5161.
[52] Yoshida K,M Okamoto,J Sasaki et al. Clinical outcome of osteosarcoma and its correlation with programmed death-ligand 1 and T cell activation markers. *Onco Targets Ther* 2019;12: 2513-2518.
[53] Mendonca M S,W T Turchan,M E Alpuche et al. DMAPT inhibits NF-κB activity and increases sensitivity of prostate cancer cells to X-rays in vitro and in tumor xenografts in vivo. *Free Radic Biol Med* 2017;112: 318-326.
[54] Gil da Costa R M,C Levesque,D Bianchi-Frias et al. Pharmacological NF-κB inhibition decreases cisplatin chemoresistance in muscle-invasive bladder cancer and reduces cisplatin-induced toxicities. *Mol Oncol* 2023;17: 2709-2727.
[55] Champa D,A Orlacchio,B Patel et al. Obatoclax kills anaplastic thyroid cancer cells by inducing lysosome neutralization and necrosis. *Oncotarget* 2016;7: 34453-71.
[56] Buettner R,L X T Nguyen,C Morales et al. Targeting the metabolic vulnerability of acute myeloid leukemia blasts with a combination of venetoclax and 8-chloro-adenosine. *J Hematol Oncol* 2021;14: 70.
[57] Rugo H S,R S Finn,V Diéras et al. Palbociclib plus letrozole as first-line therapy in estrogen receptor-positive/human epidermal growth factor receptor 2-negative advanced breast cancer with extended follow-up. *Breast Cancer Res Treat* 2019;174: 719-729.
[58] Braal C L,E M Jongbloed,S M Wilting et al. Inhibiting CDK4/6 in Breast Cancer with Palbociclib, Ribociclib, and Abemaciclib: Similarities and Differences. *Drugs* 2021;81: 317-331.
[59] Zhao T,W Li,J Chen et al. Genomic variants in Fas-mediated apoptosis pathway predict a poor response to Platinum-based Chemotherapy for Chinese Gastric Cancer Patients. *J Cancer* 2021;12: 849-859.

[60] Zhao Q,X Lin, G Wang. Targeting SREBP-1-Mediated Lipogenesis as Potential Strategies for Cancer. *Front Oncol* 2022;12: 952371.

[61] Tracz-Gaszewska Z, P Dobrzyn. Stearoyl-CoA Desaturase 1 as a Therapeutic Target for the Treatment of Cancer. *Cancers (Basel)* 2019;11.

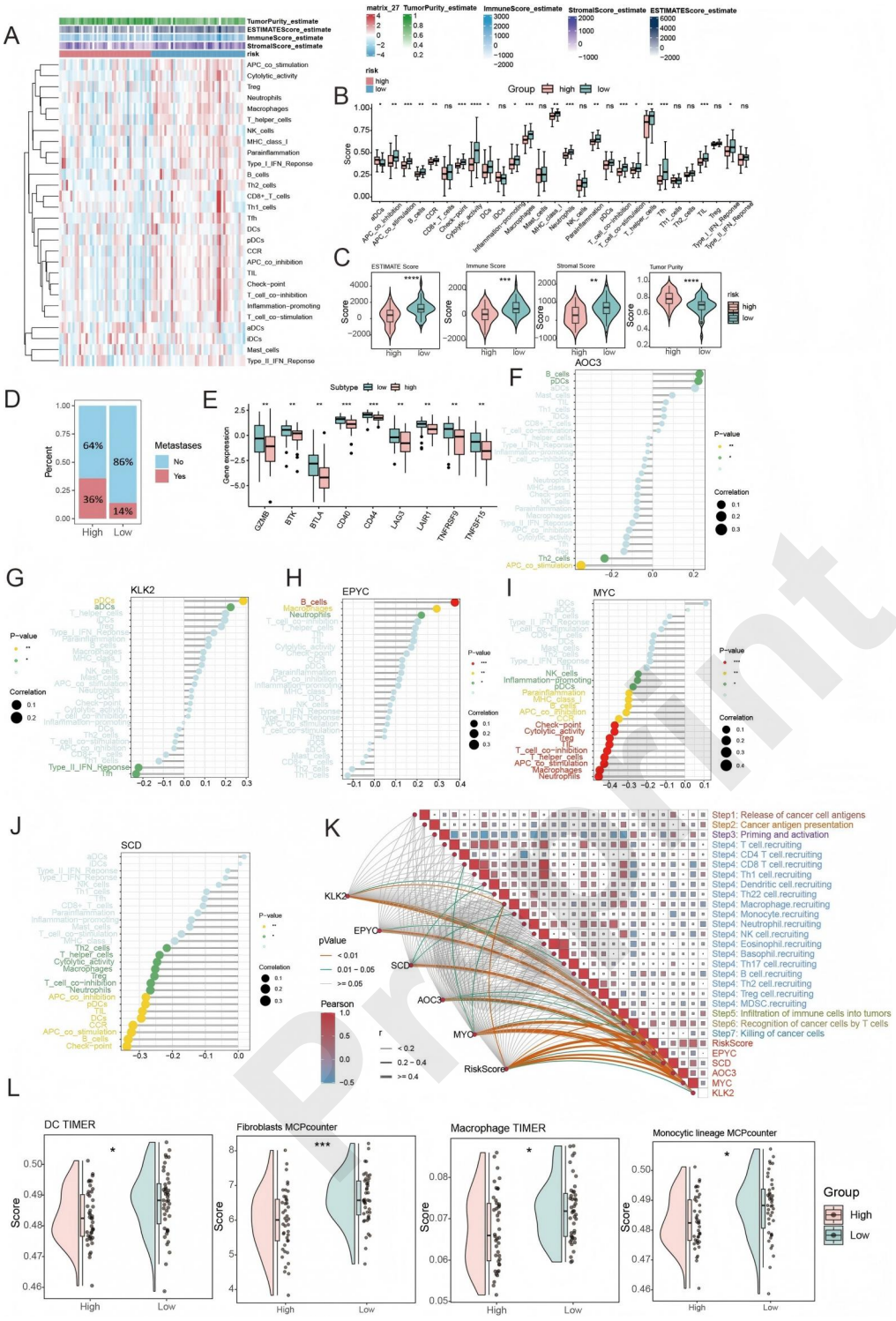
A
TumorPurity_estimate
ESTIMATEScore_estimate
ImmuneScore_estimate
StromalScore_estimate
risk
APC_co_stimulation
Cytolytic_activity
Treg
Neutrophils
Macrophages
T_helper_cells
NK_cells
MHC_class_I
Parainflammation
Type_I_IFN_Reponse
B_cells
Th2_cells
CD8+_T_cells
Th1_cells
Tfh
DCs
pDCs
CCR
APC_co_inhibition
TIL
Check-point
T_cell_co-inhibition
Inflammation-promoting
T_cell_co-stimulation
aDCs
iDCs
Mast_cells
Type_II_IFN_Reponse
B
Group high low
Score
C
ESTIMATE Score
Immune Score
Stromal Score
Tumor Purity
risk high low
D
Percent
64%
36%
86%
14%
Metastases
No
Yes
High Low
E
Subtype low high
Gene expression
GZMB BTK BTLA CD40 CD44 LAG3 LAIR1 TNFRSF9 TNFSF15
F
AOC3
P-value
Correlation
G
KLK2
H
EPYC
I
MYC
J
SCD
K
Step1: Release of cancer cell antigens
Step2: Cancer antigen presentation
Step3: Priming and activation
Step4: T cell.recruiting
Step4: CD4 T cell.recruiting
Step4: CD8 T cell.recruiting
Step4: Th1 cell.recruiting
Step4: Dendritic cell.recruiting
Step4: Th22 cell.recruiting
Step4: Macrophage.recruiting
Step4: Monocyte.recruiting
Step4: Neutrophil.recruiting
Step4: NK cell.recruiting
Step4: Eosinophil.recruiting
Step4: Basophil.recruiting
Step4: Th17 cell.recruiting
Step4: B cell.recruiting
Step4: Th2 cell.recruiting
Step4: Treg cell.recruiting
Step4: MDSC.recruiting
Step5: Infiltration of immune cells into tumors
Step6: Recognition of cancer cells by T cells
Step7: Killing of cancer cells
RiskScore
EPYC
SCD
AOC3
MYC
KLK2
pValue
Pearson
r
L
DC TIMER
Fibroblasts MCPcounter
Macrophage TIMER
Monocytic lineage MCPcounter
Score
High Low
Group
High
Low